*Laser and Particle Beams* (2002), *20*, 303–316. Printed in the USA.

DOI: 10.1017/S0263034602202220

# Recent advances in laser–plasma experiments using foams

TOM HALL,[1] DIMITRI BATANI,[2] WIGEN NAZAROV,[3] MICHEL KOENIG,[4] AND ALESSANDRA BENUZZI[4]

[1]Department of Physics, University of Essex, Colchester, CO4 3SQ, England, U.K.
[2]Dipartimento di Fisica "G. Occhialini," Università degli Studi di Milano Bicocca and INFM, Piazza della Scienza 3, 20126 Milano, Italy
[3]Department of Chemistry, Carnelley Building, University of Dundee, Dundee, DD1 4PR, Scotland, U.K.
[4]Laboratoire pour l'Utilisation des Lasers Intenses, CNRS, Ecole Polytechnique, 91128 Palaiseau, France

(RECEIVED 16 November 2001; ACCEPTED 5 February 2002)

**Abstract**

The paper discusses recent advances in the use of foams in laser–plasma experiments, concerning in particular: (1) the use of foam in order to get an efficient smoothing of laser energy deposition, (2) the problem of hydrodynamics of layered foam-payload targets, (3) the use of foam for shock pressure amplification in equation-of-state experiments, (4) the study of the equation of state of foams in the Megabar regime, and (5) the use of foams for astrophysics relevant experiments, here in particular shock acceleration experiments.

**Keywords:** Equation of state; Foam targets; Laboratory astrophysics; Laser produced plasmas; Radiation smoothing; Shock waves

## 1. INTRODUCTION

Recently, low density porous materials, or "foams," have found many applications in laser–plasma experiments and have led to the study and/or the discovery of interesting physical phenomena. On one side, such applications are related to the study of basic physical and astrophysical phenomena (Massen *et al.*, 1994; Remington *et al.*, 1997; Drake *et al.*, 1998; Koenig *et al.*, 1998). On the other side, they are related to their possible use in the context of inertial confinement fusion (ICF; Desselberger *et al.*, 1995; Dunne *et al.*, 1995; Hoarty *et al.*, 1997; Batani *et al.*, 1998). In this framework, the present article discusses some recent advances in the use of foams in laser–plasma experiments, concerning in particular: (1) the use of foam in order to get an efficient thermal smoothing of laser energy deposition in ICF (Dunne *et al.*, 1995; Batani *et al.*, 2000), (2) the problem of hydrodynamics of layered foam-payload targets (Dunne *et al.*, 1995; Benuzzi *et al.*, 1998*b*; Nazarov *et al.*, 1998; Batani *et al.*, 1999, 2000), (3) the use of foam for shock pressure amplification in equation-of-state experiments (Batani *et al.*, 2001), (4) the study of the equation of state of foams in the Megabar regime (Holmes, 1991, 1994; Koenig *et al.*, 1999*a*), and (5) the use of foams for astrophysically relevant experiments, here, in particular, for shock acceleration experiments (Koenig *et al.*, 1999*b*).

It is important to point out that all these aspects are directly related to foams which are made of low-$Z$ elements (i.e., plastic foams) only and which give origin to overcritical plasmas, or plasmas whose electronic density $n_e$ is larger than the laser critical density $n_c$. The relation

$$n_e = \rho N_A Z/A < n_c = 1.1 \cdot 10^{21}/\lambda^2 \quad (1)$$

fixes a minimum value of the mass density $\rho$ if we assume a complete ionization of the low-$Z$ elements of the foam. For instance, in the case of the foams used in the experiments described in this article, this is $\rho \leq 12$ mg/cm$^3$ for $\lambda = 0.53$ $\mu$m. Here $N_A$ is the Avogadro number, $\lambda$ is the laser wavelength in microns, $Z$ and $A$ are the average atomic number and weight of the foam, and both $n_e$ and $n_c$ are measured in cm$^{-3}$.

Hence, in the following, we will not consider the phenomena related to the direct interaction of laser light with undercritical foam-plasmas, as well as all the experiments which involve the use of metallic foams, which have been used, for instance, to study hot electron penetration in solids.

## 2. FOAM PRODUCTION

The experiments described here used foams realized with a technique developed at Dundee University (Falconer *et al.*, 1994, 1995), which allows the production of uniform foams

Address correspondence and reprint requests to: Tom Hall, Department of Physics, University of Essex, Colchester, CO4 3SQ, England. E-mail: hallt@essex.ac.uk

with submicron pore size. This is very important because in many experiments, especially those which use agar–agar foams, the structure of the foam is very nonuniform and "spaghetti-like." Very low density foams can be produced in this way, but they rather consist of filaments separated by distances which can be much larger than the laser wavelength itself and even a relevant fraction of the laser focal spot size. Again, such very low density foams give origin to undercritical plasmas which may be useful to study the interaction of the laser beam with a very underdense plasma corona (i.e., outside the scope of the present article) but even in this case, the particular foam structure may produce many peculiar aspects of the interactions which can not obviously be extrapolated to the general case.

In our case, the foams were always part of a layered target including normal density Al, Au, or CH layers. In the case of an Al-foam target, for instance, the Al layer was some 10 $\mu$m in thickness: A thin washer was glued on its rear side and then the targets were filled with a monomer solution containing a photoinitiator, and then polymerized *in situ* using UV light. The *in situ* polymerization technique produces foams in the required position in the target without the need for machining or handling, thereby reducing the risk of damage to the foam. A wide range of densities and loading of high $Z$ elements is possible using this technique. Foams densities from 5 to 900 mg/cm$^3$ can be produced by this technique, depending on the geometry of the target. The polymerization is a free-radical process and produces foams that are homogeneous with uniform submicron pore sizes (see Fig. 1). The height of the washer glued onto the Al layer fixes the thickness of the foam layer, since it is filled to the edge.

The monomer used in the experiments described here was TMPTA (trimethylol propane triacrylate, with gross chemical formula $C_{15}H_{20}O_6$), the solution for polymerization was Brij® 30 (polyoxy-ethylene lauryl (4) ether) and the initiator was benzoin methyl ether. All of these chemicals were supplied by Aldrich Chemical Company. Brij 30 was chosen as a solvent for polymerization to eliminate evaporation during the polymerization step. The small size of the targets makes the surface-to-volume ratio large, and therefore evaporation of the liquid in the targets becomes significant. The UV lamp used for polymerization was an ORIEL Q 60000 lamp, equipped with a 100-W mercury lamp and a quartz fiber optic.

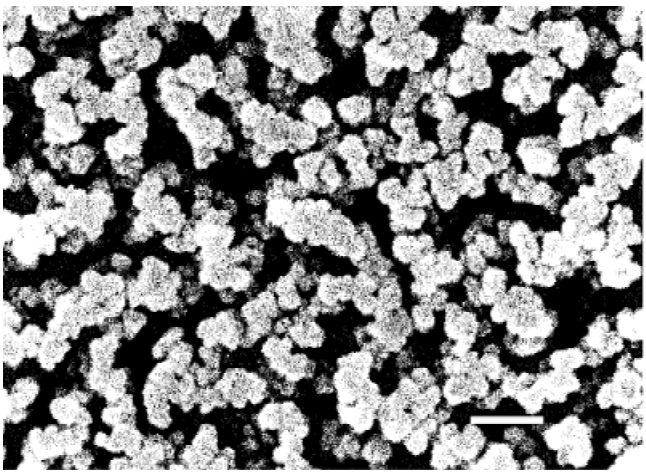

**Fig. 1.** TMPTA foam micrograph (bar = 1 $\mu$m).

The targets were placed on a microscopic stage and filled with a solution of monomer in Brij 30 using a syringe equipped with a microneedle (typically 10–20 $\mu$m tip size). The targets were then illuminated with the UV light to polymerize the monomer in the Brij 30 solution. The solution gelled in a few seconds. These targets containing the gel were precipitated in a nonsolvent such as methanol. Once the precipitation of the gel was completed, they were dried with a critical point drying (CPD) apparatus (Polaron 3100). Critical point drying is essential for the *in situ* polymerization technique. Any other drying method will damage the structure of the foam.

## 3. SMOOTHING

One of the more important reasons to use foams is related to the question of the smoothing of laser energy deposition in ICF targets. As it is well known, the problem of uniformity of energy deposition in direct-drive ICF is of the main importance in order to obtain ignition and high gain. To improve the uniformity of laser illumination, optical smoothing techniques have been introduced in the last few years, which include for instance, the use of random phase plates (Kato *et al.*, 1984), phase zone plates (Koenig *et al.*, 1994; Stevenson *et al.*, 1994; Bett *et al.*, 1995), kinoform phase plates (Dixit *et al.*, 1994), smoothing by spectral dispersion (Sckupsky *et al.*, 1989), or induced spatial incoherence (Lehmberg & Obenschain, 1983). Despite the considerable success of all such techniques, especially when used together, they are, in principle, unable to deal with the problem of laser nonuniformity at very early times during the laser–target interaction. This has been called "laser imprint" problem (Emery *et al.*, 1991; Desselberger *et al.*, 1992) and may have important consequences on compression uniformity at later times, and in particular on the development of Rayleigh–Taylor instability (Taylor *et al.*, 1996), even if optical smoothing is used.

In this context, the use of low density foams has been recently proposed as a means of improving uniformity of energy deposition (Desselberger *et al.*, 1995; Dunne *et al.*, 1995). A low density foam is inserted between the target itself (the payload material) and the laser, producing a long overcritical plasma where laser nonuniformities are homogenized by thermal smoothing. As is well known, thermal smoothing reduces the pressure variations $\delta P$, which are present at the laser deposition surface (usually the critical density layer in the plasma), by a factor

$$\Gamma = \exp(-\alpha kL), \tag{2}$$

where $k$ is the wave number of the spatial perturbations of the incident laser beam, $\alpha$ is of the order of 1, varying according to the different models (Gardner & Bodner, 1981; Manheimer *et al.*, 1982), and $L$ is the stand-off distance, that is, the distance between the laser deposition layer and the ablation front.

The "foam-buffered ICF" scheme was first realized by Dunne *et al.* (1995) in preliminary experiments using a plastic foam with density $\rho = 50$ mg/cm$^3$ and thickness $d = 50$ $\mu$m, illuminated by a laser beam at intensity $I \leq 5 \cdot 10^{14}$ W/cm$^2$. According to their results, a key element for the success of the smoothing technique is the presence of a thin gold layer ($\approx$250 Å), a "converter foil," before the foam layer. This layer, which rapidly evaporates and burns through, produces a high flux of soft X rays which drives a radiation-driven wave in the foam material, thereby ionizing the material and producing the overcritical plasma which is needed for thermal smoothing. The authors qualitatively explain their results by saying that in the case where the foam is present, the stand-off distance $L$ must be replaced by all the thickness of the foam layer, which has been transformed in an overcritical plasma layer, so that the factor $\Gamma$ is strongly decreased.

In this context we have realized some experiments in order to clarify the influence of foam parameters (density, thickness, etc.) and that of X-radiation on the effectiveness of smoothing. Also we wanted to control the laser beam nonuniformities in order to verify what is the scale of the nonuniformities which are really smoothed with the foam technique. The schematic setup of our experiment is shown in Figure 2. Its basic elements are:

1. The use of foams of density from 30 to 200 mg/cm$^3$ to study the smoothing effects as a function of foam density (instead the foam thickness was fixed at $\approx$60 $\mu$m).
2. The use of well-known nonuniformities which have been produced first by using phase zone plates to produce a smooth and flat beam profile (Koenig *et al.*, 1994), and then by inserting opaque grids before the foam. In this first experiment, only the grid with a 60-$\mu$m spacing was used.
3. The use of grids of different materials in order to change the radiation emission (concerning both the intensity and the spectral distribution of X rays). Then, in our experiment, the grid had the double role of producing the laser nonuniformities which we wish to smooth away and the radiation which should create the overcritical plasma.

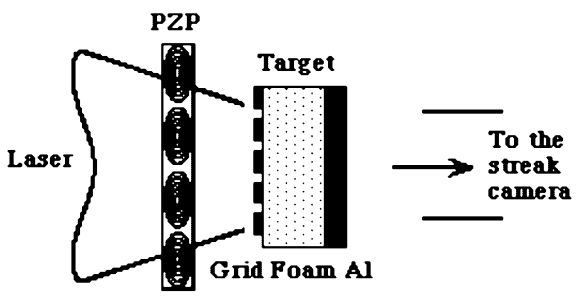


**Fig. 2.** Experimental setup for the measurement of foam smoothing.

A streak camera was used as diagnostic in the experiment to detect the shock breakout from the layered targets made of foam on the laser side and an aluminum layer on the rear side (Fig. 2). Although aluminum is not a material used in ICF foam-buffered targets, it allows us to simulate the realistic situation of shock transmission from the low density foam to a denser payload material. The great advantage of aluminum is that its EOS is well known, for instance, through the SESAME tables (T4 Group, 1983), which makes it a typical reference material in shock experiments.

The experiment was performed using three beams of the LULI Nd laser (converted at $\lambda = 0.53$ $\mu$m, with a total maximum energy $E_{2\omega} \approx 100$ J). The pulse was Gaussian in time with a full width half maximum (FWHM) of 600 ps. All beams had a 90-mm diameter and were focused with an $f = 500$ mm lens onto the same focal spot. As already said, phase zone plates (PZP) were used to eliminate large-scale spatial intensity modulations and produce a flat-top intensity profile. Since the smoothing effect introduced by the foam varies with its density, the use of PZP was necessary in our experiment in order to get the same irradiation conditions for any foam density. Our optical systems (PZP + focusing lens) produced a total focal spot of 400 $\mu$m FWHM, with an $\approx$200-$\mu$m-wide flat region in the center, corresponding to a laser intensity $I \approx 3$–$5 \cdot 10^{13}$ W/cm$^2$. Such large focal spots were needed to reduce 2D effects because the total thickness of the target was $\approx$80 $\mu$m.

The target was made with an Al layer (13.2 $\mu$m thick) and grids with spacing 30 $\mu$m and step 30 $\mu$m (except for the plastic grids, which had, respectively, 27.5 and 32.5 $\mu$m). Their thickness was 9 $\mu$m and they were realized in different materials, that is, gold, copper, and plastic (this last to produce a small X-ray flux and low radiative effects in the foam).

Figure 3 shows streak images obtained with foams of density 30 and 200 mg/cm$^3$ and Cu grids. We see a time fiducial on the top-left of each image. In contrast, Figure 4 shows results obtained for 50 mg/cm$^3$ and different grid materials. They show how smoothing is affected both by the grid material and the foam density.

Two features seem at first surprising: First a foam density of 30–50 mg/cm$^3$ seems to produce better smoothing than a 100–200-mg/cm$^3$ foam, although a denser plasma will certainly be formed in this last case; and second, the smoothing effect seems better in copper as compared to gold, while gold is known to have a higher laser-to-X-rays conversion efficiency.

We think that the first result points out how it is not only the foam density that plays a role in the smoothing effect, that is, the fact that the plasma formed is overcritical. Also

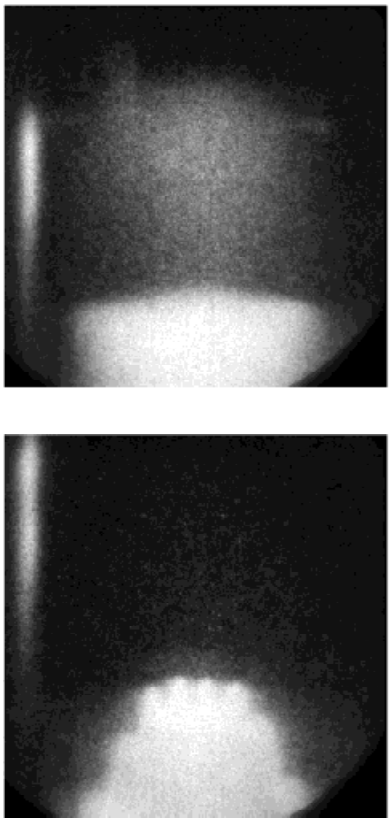


**Fig. 3.** Streak camera images with foams of density 30 (a) and 200 mg/cm$^3$ (b) and Cu grids. The laser energies were 92 and 94 J.

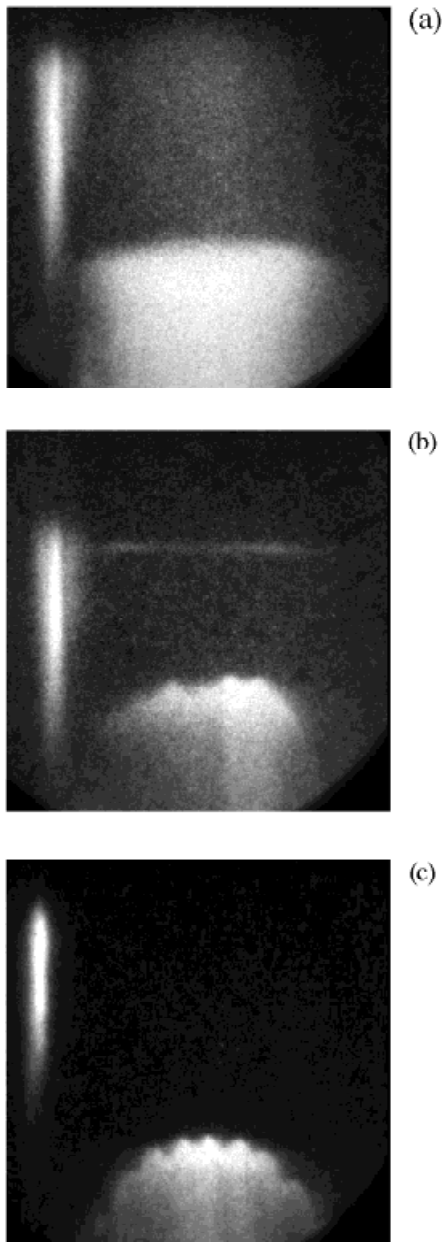


**Fig. 4.** Streak camera images for $\rho = 50$ mg/cm$^3$ and different grids: Cu (a), Au (b), CH (c). The laser energy was, respectively, 94, 90, and 79 J.

its temperature is very critical and the temperature is inversely proportional to the heated mass, that is, to the number of heated particles or foam density. A higher temperature will increase the electron mean free path and lateral energy losses, thereby contributing to a more effective thermal smoothing. This can easily be seen by looking at the formula for thermal conduction which scales versus temperature as $T^{5/2}$, and justifies the fact that smoothing is more effective at 30–50 mg/cm$^3$ than at 100–200 mg/cm$^3$. In this last case, indeed, we could calculate that the temperatures reached in the plasma are a factor of 2 to 4 lower than with 30–50 mg/cm$^3$.

The second result is due to the different X-ray spectra of Cu and Au. Although conversion efficiency is lower in Cu, its spectrum extends to higher X-ray energies (Eidmann & Kishimoto, 1986; Mochizuki *et al.*, 1986; Chaker *et al.*, 1988). Such "hard" photons may penetrate easily to the Al layer and preheat it. The observed better smoothing which is obtained with Cu as compared to Au is, hence, probably the indirect effect of the stronger preheating induced in Al in the case of Cu. Target preheating obtained with Cu produces a change in Al, thereby strongly increasing the thermal smoothing effectiveness in the Al heated layer. It must be recalled, indeed, that the thermal smoothing effect observed at the target rear side through shock wave detection does correspond to the whole foam + Al layers. However the situation with Cu is worse with respect to its applicability to the idea of foam-buffered ICF. Indeed, it is true that target preheating must be avoided in ICF since it will move the target material off the isentrope with a significant loss of compression efficiency. The effective thermal smoothing in the foam layer alone is probably about the same with Cu and Au, since in both cases, plasmas of similar density and temperature are produced (with a slightly preference towards the use of Au).

Our results point out the importance of carefully choosing the foam and the converter foil parameters (in particular foam density and foil material). Of course it is not immediately possible to extrapolate our case, in which the grid acts both for the introduction of nonuniformities and the gener-

ation of X rays, to the case where a real converter foil is used. Anyway, all the qualitative aspects connected to the shape of the X-ray spectrum, observed in our experiment, remain, of course, valid in the other case.

At the same time, we clearly showed how thermal transport in the overcritical plasma produced in a low density foam by X-ray irradiation ("radiation driven") allows a smoothing of laser-imprints nonuniformities of the order of 100%. This is true even with the very large scale of nonuniformities used in our experiment (≈60 $\mu$m from peak to peak) and will be obviously easier in the case of smaller nonuniformities, which are more easily smoothed by thermal transport.

## 4. HYDRODYNAMICS

Despite the encouraging results on foam smoothing obtained both in Dunne *et al.* (1995) and in Batani *et al.* (2000), the smoothing capability of foams is not the only critical parameter in assessing the real applicability of foam-buffered targets to ICF. Indeed the introduction of foams should not create a plasma where laser instabilities are likely to develop, and also the hydrodynamics of such foam-buffered targets should be studied to verify that no appreciable degradation of the laser–target coupling, that is, of the compression efficiency of the pellet, occur.

The last problem has been considered in Dunne *et al.* (1995), but the diagnostics used in the experiment allowed the study of the hydrodynamics of a layered foam-solid targets at late times only. The authors did show that the time histories of the target motion with and without a foam layer were substantially the same, but this is exactly what is to be expected since the target motion at long times is determined only by its mass (which does not change much because of the foam layer) and by the laser ablation pressure, which is relatively independent of the ablated material as expected from simple models (Fabbro, 1982; Mora, 1982; Lindl, 1995).

Moreover, the details of shock propagation in foams and the transmission of the momentum to the payload material also need to be studied. Indeed, in ICF, it is very important to minimise the drive energy by compressing the target along a low isentrope and reach a high gain. Thus the generation of too strong a shock, which could preheat the thermonuclear fuel and make its compression more difficult, must be avoided, especially in the early stage of the implosion (Emery & Gardner, 1992).

Hence more precise diagnostics are needed to study how the target is set in motion and not only its motion at late times. To this particular end we have studied the influence of introducing a foam layer on laser-produced shock, studying the shock breakthrough from layered targets made of a foam layer on the laser side and a stepped aluminum layer on the rear side. A streak camera was used to detect shock breakthrough at the base and at the step of the aluminum target, allowing the shock velocity to be determined. Again, aluminum is not a realistic payload material for ICF targets, but it is useful since its EOS is well known. The schematic experimental setup is shown in Figure 5.

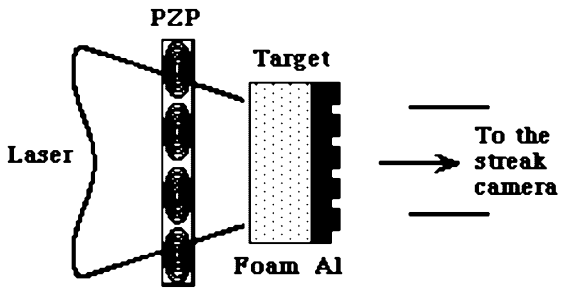


**Fig. 5.** Experimental setup for the measurement of shock amplification.

The characteristics of the focusing system and the laser are as given in the previous section. The stepped Al targets were produced at the Target Preparation Laboratory in CEA–Limeil with an electron gun deposition technique (Faral *et al.*, 1994). The accurate target fabrication technique allowed sharp step edges to be obtained and a precise determination of step heights. The aluminum base thickness was in the range of 10 to 12 $\mu$m, and the step in the range of 4 to 6 $\mu$m.

Figure 6 shows two streak camera images. In both cases, it is possible to see a time fiducial on the top-right of the image obtained by sending a portion of the laser beam onto the streak camera slit with an optical fiber. In Figure 6a, a stepped aluminum target without foam was used while in Figure 6b, a foam layer was present on the laser side. All the other conditions, including laser pulse energy ($E_{2\omega} \approx 32$ J), were the same.

Such pictures show a delayed shock breakthrough, that is, a longer time between the maximum of the laser pulse (measured through the time fiducial) and shock arrival when the foam is present. This corresponds to the time needed for the

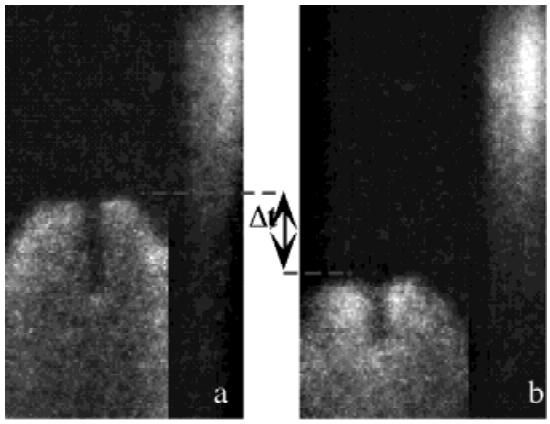


**Fig. 6.** Streak images: (a) stepped aluminum target (base 13 $\mu$m, step 5 $\mu$m), (b) same target with a foam layer ($\rho = 50$ mg/cm$^3$) on laser side. The shock velocity is 18 km/s for (a) and 31 km/s for (b). The flat shock region is ≈200 $\mu$m large. The time delay, $\Delta t$, is 410 ps.

shock to travel through the thick foam. The pictures also show that the shock velocity inside the aluminum target, and hence the pressure generated in aluminum, increases. The values of pressure have been deduced from shock velocity by using the SESAME tables (T4 Group, 1983).

Such effects have been found to be a function of the foam density and thickness as shown in the experimental results of Figure 7. The points corresponding to $\rho = 1$ are those obtained with stepped targets without foam. The pressure generated in this last case (≈7 Mbar, on average) corresponds approximately to what can be obtained from scaling laws (Fabbro, 1982; Mora, 1982; Lindl, 1995) for our laser and target parameters:

$$P_0 \approx 8.6(I_L/10^{14})^{2/3}\lambda^{-2/3}(A/2Z)^{1/3}. \quad (3)$$

The points for $\rho = 900$ mg/cm$^3$ correspond to targets which have a layer of polymer at normal density. Here the plastic thickness is 15 $\mu$m; indeed the use of a 60-$\mu$m layer in this case would have implied the shock pressure is not maintained, our laser pulse duration being too short.

The explanation of our experimental results relies on an impedance mismatch between foam and aluminum. At the arrival of the shock wave at the interface, a shock is transmitted in aluminum and another one is reflected into the foam. The different materials on the two sides have the same pressure and fluid velocity, this common point being at the intersection of the aluminum shock polar and the foam polar for reflected shocks (Zeldovich & Raizer, 1967). By decreasing the foam density, the impedance mismatch between the two materials increases and one would expect that the shock pressure in aluminum would become bigger. We note, however, in Figure 7 that for foam densities $\rho \approx 100$ mg/cm$^3$, the behavior is reversed and the pressure decreases. Several effects contribute to produce this result. First, at the lowest densities, it is not possible to avoid the direct interaction of the laser beam with the metal target behind the foam. This is due to the fast ablation rate of the foam and also to the fact that the foam itself may be undercritical. Simple analytical laws predict the ablation rate (Mora, 1982) as

$$dm/dt = 4.5\cdot 10^{-6} I^{3/4}\lambda^{-1/2}t^{-1/4}, \quad (4)$$

where $\lambda$ is in microns, $t$ in nanoseconds, $I$ in watts per centimeter squared, and $dm/dt$ is in units of g cm$^{-2}$ s$^{-1}$. Hence the ablation rate (and the shock pressure) are independent of the foam density, and the ablation velocity is inversely proportional to it, giving for our laser parameters a limit of about $\rho \geq 15$ mg/cm$^3$. Foams with lower density are completely ablated during the pulse.

Furthermore, a direct laser–metal interaction takes place with undercritical foams, that is, if $\rho \leq 12$ mg/cm$^3$ in case of total ionization. A partial ionisation is not likely, considering the high temperatures reached in the foam (as shown in numerical simulations), but it would mean that an even higher foam density would be required to reach critical density. These two effects contribute to gradually lower the shock pressure to the value measured in simple metal targets, hence producing a meaningful continuity of physical results. The residual measured pressure increment for such low densities is probably due to the partial confinement of the expanding aluminum plasma by the foam, as observed in shocks produced from focusing lasers on the surface of targets immersed in water or under a layer of transparent material (Fabbro *et al.*, 1990).

For the denser foams, in the range of 20 to 100 mg/cm$^3$, the pressure generated at the interface is increased due to impedance mismatch, but other effects arise which justify the behavior of shock pressure versus foam density:

1. First, the shock is initially accelerating and, therefore, it may transmit to the aluminum layer before maximum pressure has been reached. By using shock relations for ideal gases, it is possible to show analytically that in this case, for a fixed foam thickness the pressure generated in aluminum decreases with density.
2. Second, the pressure generated at the interface is not maintained due to the fast transit times of the reflected shock followed by the unloading wave. The laser intensity sustains a pressure given by Eq. (3) in the foam, which is then increased in the aluminum due to the impedance mismatch. The reflected shock travels rapidly back through the foam and is then reflected as an unloading wave at the critical surface. This unloading wave will also travel rapidly through the hot foam and aluminum and may reach the initial shock in the aluminum before this breaks out from the rear surface. This effect results in a decrease in the pressure inside the metal as a function of time, and so we measure a shock velocity which is smaller than that which corresponds to the maximum pressure determined by the impedance mismatch conditions. Moreover, the experiment measures the average velocity inside the step,

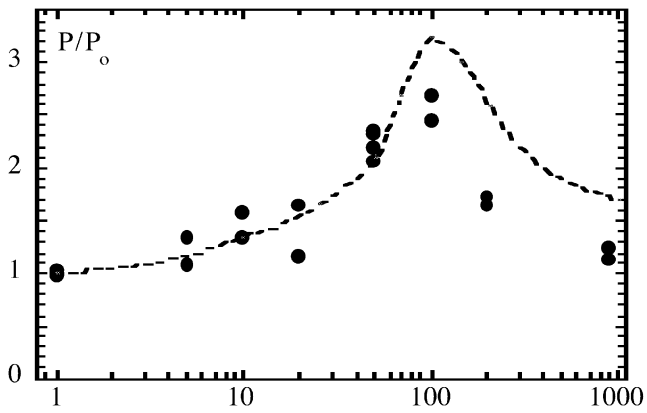


**Fig. 7.** Amplification of pressure obtained in aluminum versus foam density $\rho$ in (mg/cm$^3$). $P_0$ is the value for simple aluminum targets. Also shown are the results of MULTI simulations.

hence giving a lower velocity than at the bottom of the step.

To simulate our data, we used the hydrocode MULTI (Ramis *et al.*, 1988). Simulations clearly show that for densities below 100 mg/cm$^3$, a very high pressure is reached at the aluminum–foam interface, but it is not maintained, and begins quickly to decay as the relaxation wave from the ablation front reaches the slower shock propagating in the aluminum. The simulation results, shown in Figure 7, are affected by radiation transfer. Radiative effects are evidenced in the simulations, as already described in literature (Zeldovich & Raizer, 1967; Massen *et al.*, 1994), but in our case, the effects are significant but not dominant. By comparison with an equivalent mass of normal plastic, the foam is heated to higher temperatures by the compression and also, being very low density, is more transparent to radiation. Hence, even though not much XUV radiation is produced (foams being made of low $Z$ elements only), preheating ahead of the shock front is nonnegligible. Moreover, because of the higher temperatures and higher transparencies of the foam relative to normal plastic, the interface between foam and metal will preheat more since radiation propagating in the foam will be stopped due to the much higher absorption in the metal. So a slight modification of the plasma profile is expected at the interface.

It is also evident that while the simulations describe the overall behavior of experimental data qualitatively well, the fine details are not explained. In particular, from MULTI, for the plastic at normal density, we find a value of $P/P_0 \geq 1.75$ in agreement with what can be deduced from impedance mismatch relations in the perfect gas approximation

$$P/P_0 = 4\rho_{\mathrm{Al}}/(\sqrt{\rho_{\mathrm{Al}}} + \sqrt{\rho})^2 \tag{5}$$

where $\rho_{\mathrm{Al}} = 2.7$ g/cm$^3$ and $\rho = 0.9$. The lack of detailed agreement may be, in part, connected to the fact that foam opacities (and foam EOS) are not sufficiently well known. We have used the Los Alamos opacity data (Cohen & Clark, 1996) and the SESAME EOS for plastic, where we have taken into account the initial low foam density.

Finally the computer simulations used to interpret our experimental results show that, at least in the first approximation, the ablation pressure is independent of foam density and equal to that in aluminum. This shows again that target motion at late times, as studied in Dunne *et al.* (1995) is not enough to discriminate the effects due to the presence of the foam.

We conclude that shock propagation in foam is a complex hydrodynamic phenomenon and that at foam–solid boundaries, a key role is played by the pressure increase due to the impedance mismatch. We have shown how the presence of a foam layer can strongly increase the pressure reached in an adjacent metal layer. Our results have important consequences for the design of foam-buffered targets which have been proposed for ICF to remove the initial imprint by radiative smoothing. Shock enhancement at the foam–solid boundary will move the target material off the isentrope with a consequent loss of compression efficiency.

## 5. SHOCK AMPLIFICATION

The "negative" shock pressure amplification effect described in the previous section may be "positively" exploited for EOS experiments. The study of equation of states of matter in high pressure conditions (above 10 Mbar) is a subject of great interest for several fields of modern physics. In particular, it is important in the context of astrophysics and inertial confinement fusion research. Some EOS already exist for this pressure range (T4 Group, 1983), but, first, they mainly come from calculations and theoretical models, with only a few experimental data available to validate them, and furthermore they exist for a restricted number of materials. Therefore the behavior of many materials under high pressure is still unknown. In the past, EOS measurements in the tens of megabars domain could be performed only by nuclear explosions. Nowadays, it is possible to reach very high pressures in laboratories by using powerful pulsed laser-generated shock waves in solid material. Early experiments have shown the possibility of producing shock waves with pressures up to 100 Mbar in a laser-irradiated solid (van Kessel & Sigel, 1974; Trainor *et al.*, 1978; Veeser & Solem, 1978; Cottet *et al.*, 1984, 1985) and in a target foil impacted by a laser-accelerated foil (Obenschain *et al.*, 1983; Fabbro *et al.*, 1986; Faral *et al.*, 1990). Pressures as high as 750 Mbar were achieved by using laser pulses of 25 kJ (at wavelength $\lambda = 0.53$ $\mu$m) and a foil impact technique (Cauble *et al.*, 1993). However, in many of these experiments, the bad quality of shocks prevented them from being used as a quantitative tool in high pressure physics.

Planarity and stationarity of the shock fronts, as well as low preheating of the material ahead of the shock waves, are essential to obtain accurate measurements of EOS. Recent experiments (Koenig *et al.*, 1994; Lower *et al.*, 1994; Batani *et al.*, 1995) have proved the possibility of creating spatially very uniform shocks in solids either by using direct laser drive with optically smoothed laser beams or X-ray thermal radiation (indirect laser drive).

Once high quality shocks are obtained, it is possible to perform precise measurements of the shock parameters. In particular, EOS points can be obtained if two quantities of the shocked material, related to the Hugoniot–Rankine relations (Zeldovich & Raizer, 1967), are measured simultaneously. In a recent experiment (Collins *et al.*, 1998), the simultaneous measurement of two parameters (the shock velocity $D$ and the fluid velocity $U$) has been applied to the measurement of the EOS of deuterium. The main problem connected with this method is that it is necessary to use high energy laser pulses with the aim of maintaining a constant

ablation pressure for a few nanoseconds and of irradiating large target areas. Another method for the determination of EOS points is based on the impedance-matching technique and consists in measuring the shock velocity simultaneously (on the same laser shot) in two different materials. This makes it possible to achieve a relative determination of one EOS point of one material by taking the EOS of the other one as a reference. The reliability of this method, used in the past in nuclear experiments, has been recently proven in laser-driven shock experiments (Batani *et al.*, 1995; Koenig *et al.*, 1995) and applied to EOS measurements for Cu (Benuzzi *et al.*, 1996), and doped plastics (Koenig *et al.*, 1998). Such a method has the advantage that high pressures (10–50 Mbar) can be reached with lasers of relatively small size ($\approx$100 J).

However, the limited energy of the laser, combined with the request of having almost 1D shocks (and, hence, relatively large focal spots) fixes an upper limit to the pressure which can be obtained in the material. On the other side, even if a very big laser system is available, the laser intensity on target cannot be increased indefinitely. Indeed higher intensities mean a higher plasma temperature and, hence, larger X-ray generation in the corona. Also, above a certain intensity threshold, laser instabilities like two-plasmon-decay (TPD) and stimulated Raman scattering (SRS) can take place in the plasma corona leading to an important production of hot electrons. Such nonlinear physical phenomena take place at laser intensities of the order of $10^{14}/\lambda^2$ W/cm$^2$ where $\lambda$ in microns is the laser wavelength. Since hard X rays and hot electrons are the principal causes of preheating of the material ahead of the shock wave, it is clear that intensities on target above this limit must be avoided.

A practical way of reducing X-ray emission is the use of a low $Z$ ablator (e.g., plastic) before the target material. Luckily enough, this also proves to be a way to increase shock pressure due to the well-known impedance mismatch effect at the ablator–target interface (Zeldovich & Raizer, 1967). In passing, we notice that the impedance-matching technique was used largely in the past to intensify laser-driven shock waves (Obenschain *et al.*, 1983; Fabbro *et al.*, 1986; Faral *et al.*, 1990).

Such effect can be maximized by using low density foams before the laser target, as seen in the previous section. However shock stationarity is essential in this case which means that (1) the shock must be transmitted from foam to the payload material after it has become stationary, and (2) the shock must emerge from the rear side before it has been reached by the relaxation wave. The first condition fixes a minimum thickness for the foam and the second one a maximum thickness. Between these two values, shock stationarity is assured. Simple analytical models and computer simulations can predict both the shock pressure increment and this stationarity range.

This experiment was performed using the Asterix laser facility at the Max Planck Institut fur Quantenoptik in Garching (MPQ). It delivers a single beam, of diameter 30 cm, with an energy of 250 J per pulse at a wavelength of 0.44 $\mu$m. The temporal behavior of the laser pulse is Gaussian with a FWHM of 450 ps. The schematic experimental setup is, of course, the same as that described in the previous section (see Fig. 5). The laser beam was focused directly onto the target with an $f = 564$ mm lens. The design of the PZP had Fresnel lenses of 2.5 cm diameter, which implies that 144 Fresnel lenses are covered by the laser beam. The characteristics of our optical system (PZP + focusing lens) were such that we produced a total focal spot of 400 $\mu$m FWHM, with a 250-$\mu$m-wide flat region in the center, corresponding to a laser intensity $I \leq 2 \cdot 10^{14}$ W/cm$^2$. Such large focal spots were needed to reduce 2D effects, because the total thickness of the target could even be of the order of 170 $\mu$m.

The diagnostic used to detect the shock emergence from the target rear face consisted of an $f = 100$ mm objective imaging the rear face onto the slit of a streak camera, working in the visible region. The temporal resolution was better than 8 ps and the imaging system magnification was $M = 10$, allowing a spatial resolution better than 10 $\mu$m. A protection system was used for the diagnostics light path, to shield the streak camera from scattered laser light. The main difference with the experiment performed at LULI was that here both the foam density and foam thickness were changed (this last in the range 50 to 150 $\mu$m). Also the payload material was gold instead of aluminum.

Figure 8 shows the obtained experimental results, together with the theoretical prediction obtained with a simple analytical model (Batani *et al.*, 2001). It is evident that, apart from low thickness corresponding to an initial phase of shock formation, the pressure increase can effectively be stationary.

The pressure increase due to impedance mismatch at the payload–foam interface was measured experimentally and pressures higher than 60 Mbar were achieved in gold. Sta-

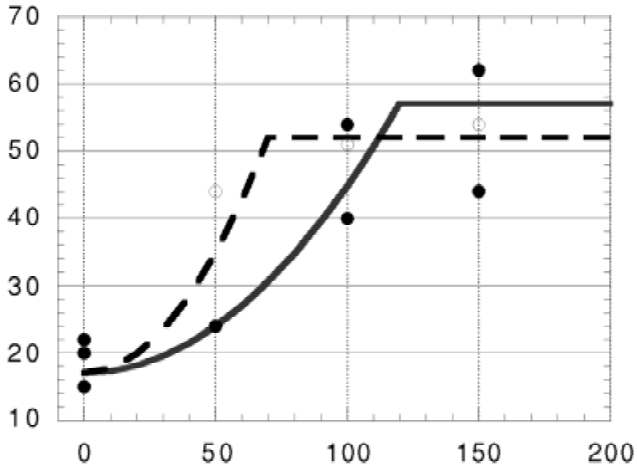


**Fig. 8.** Experimental results obtained at MPQ for shock amplification: pressure in megabars (vertical axis) versus foam thickness in microns (horizontal axis) for foams with density 20 mg/cm$^3$ (black circles) and 50 mg/cm$^3$ (white circles).

tionarity is achieved on shorter foam thickness for a bigger density since here shock velocity is lower, but a smaller density means a larger shock amplification. Increments of a factor ≈4 in shock pressure have been demonstrated. Due to the weak scaling of pressure versus laser intensity (see Eq. (3)) this would require a factor ≈10 increment in intensity on target for which a few kilojoule laser would be necessary. Also this would imply the use of intensities falling in the nonlinear regime where preheating can become quite dangerous.

There is, however, a limit to the pressure amplification which can be obtained for a given base material (the reference material in EOS experiment). From Eq. (5), this corresponds to the limit $\rho \to 0$ or $P/P_0 = 4$.

To reach this maximum, the conditions on foam thickness previously recalled must be fulfilled and also a laser focal spot with a radius larger than the total target thickness must be used in order to avoid 2D effects.

Our results may open the way to the use of foams in EOS experiments as a relatively easy way of relaxing laser energy requirements. Hence foams can increase the efficiency of direct drive EOS experiments (already more efficient than X-ray indirect drive) allowing very high pressures to be reached with relatively small laser systems.

## 6. EQUATION OF STATE

The lack of precise agreement between numerical simulations and experimental results shown in Figure 7 can be, in part, ascribed to the nonprecise knowledge of the EOS of foams. Also the design of foam-buffered ICF targets would require the precise knowledge of their EOS. However, until very recently, only very few data related to EOS were available (Holmes, 1991, 1994). Hence we decided to perform some EOS measurements of foams using laser-driven shock waves. These measurements required a target design which allowed simultaneous determination of shock velocities in a reference material (aluminum) and in the foam. Data were obtained for a wide range of densities, from 20 mg/cm$^3$ up to 1.1 g/cm$^3$.

The experiment was performed at LULI, with the characteristics already detailed in the previous sections. The target scheme is shown in Figure 9. The layered targets were made of an aluminum layer on the laser side, coated with 3 $\mu$m of plastic in order to reduce hard X-ray preheating effects (Hall *et al.*, 1997; Benuzzi *et al.*, 1998*a*). A stepped aluminum layer was then deposited on the rear side. The aluminum base thickness was in the range of 9 to 10 $\mu$m, and the step in the range of 5 to 6 $\mu$m. Then a thin washer (≈20 $\mu$m) was glued on the rear side and was filled with foam.

Foams, ranging in density from 20 to 400 mg/cm$^3$, with uniform submicron pore sizes, have been used in these experiments. Also, for complete comparison with plastic EOS models, we used TMPTA plastic at its normal density (1.1 g/cm$^3$). The brass ring height determined the final thickness of the foam, which was precisely measured by optical microscopy before each shot. A thin aluminum layer

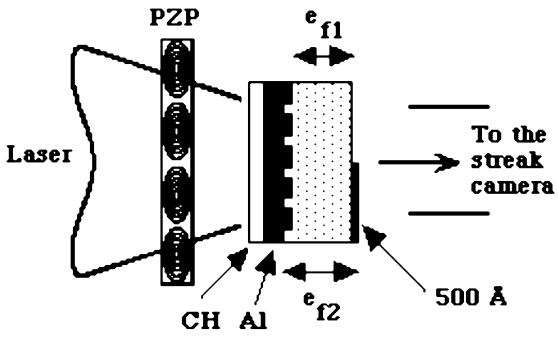


**Fig. 9.** Schematic diagram of the target for the EOS measurements.

(500 Å) was deposited on one-half of the target rear side in order to avoid shinethrough of the shock breakout from the aluminum base and steps. Since the foam is transparent to visible light, this target scheme allows us to detect, on the same shot, the shock breakout from the aluminum base and steps and from the rear surface of the foam.

As usual, the shock breakout from the target was inferred by detection of the emissivity of the target rear face in the visible region.

Our experiment is based on the impedance-matching technique applied to the "double-step targets" sketched in Figure 9. The washer glued on the rear side, filled in with the foam, allows us to have two steps with different thicknesses $e_{1f}$ and $e_{2f}$. With these two thicknesses, we were able to check if the shock is stationary during its propagation through the foam. Using rear-face, time-resolved imaging, we experimentally determined the velocity of the shock propagating through the step of aluminum $D_{\mathrm{Al}}$ and through the two foam thicknesses, $D_{1f}$ and $D_{2f}$, respectively. These shock velocities correspond to particle velocities $U_{\mathrm{Al}}$, $U_{1f}$, and $U_{2f}$, respectively, as seen in Figure 10.

In our case, since foam has a lower density than aluminum, an unloading wave is reflected in the aluminum when the shock goes through the interface between the two materials. The propagation of this wave is governed by an isen-

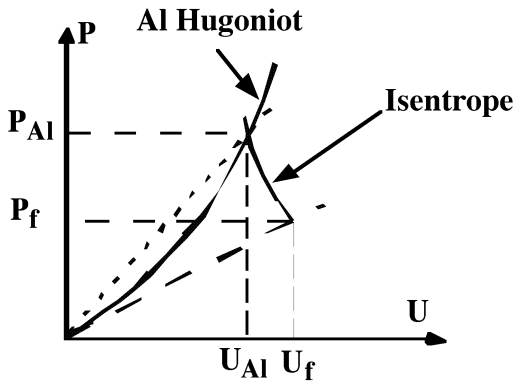


**Fig. 10.** Principle of the EOS measurement: short dashed line (- - -): $\rho_{\mathrm{Al}} D_{\mathrm{Al}} U$, longer dashed line (– – –): $\rho_f D_f U$.

tropic flow originating from the point $(P_{\mathrm{Al}}, U_{\mathrm{Al}})$, (see Fig. 10), which is given by (Zeldovich & Raizer, 1967)

$$U(P) = U_{\mathrm{Al}} - \int (-\partial V/\partial P')^{1/2} dP' \qquad (6)$$

where the integral is made on the constant entropy path between $D_{\mathrm{Al}}$ and $D$. Since the aluminum EOS is well known up to 40 Mbar, we could thus determine the isentropic curve corresponding to the passage at the aluminum–foam interface. Therefore the intersection of this release curve in the $(P, U)$ plane with the line of slope $\rho_f D_f$ ( $\rho_f$ and $D_f$ being the foam initial density and shock velocity, respectively) gives a point $(P_f, U_f)$ on the foam EOS.

Note that the impedance mismatch method, applied in shock EOS experiments, normally allows us to obtain data for an unknown material which is denser than the reference material. Instead, with this technique, first used in Koenig *et al.* (1998), EOS data can be obtained also for material of lower densities.

Figure 11 shows a typical streak camera image obtained in our experiment. The time interval $\Delta t_1$ corresponds to the travelling time of the shock through the aluminum step, thus giving $D_{\mathrm{Al}}$ by knowing the step thickness. $\Delta t_2$ and $\Delta t_3$ are the transit times of the shock through the large and small thicknesses of foam $e_{1f}$, $e_{2f}$, respectively (see Figs. 9 and 11). Here $\Delta t_1$ is $261 \pm 5$ ps, which gives a shock velocity of $21 \pm 0.8$ km/s. Using the aluminum SESAME EOS table, this corresponds to a pressure $P_{\mathrm{Al}} = 7 \pm 0.6$ Mbar.

As a result of the target design, we have two measurements of the shock velocity in the foam given by $\Delta t_2$ ($987 \pm 7$ ps) and $\Delta t_3$ ($846 \pm 9$ ps). The related shock velocities, corresponding to Figure 11, are $29.6 \pm 1.6$ km/s and $28.1 \pm 1.6$ km/s, respectively. These data imply that the shock speed is nearly constant in the foam with possibly a slight increase at the end of the largest thickness (i.e., the assumption of a constant velocity is compatible with our experimental errors). To assess this argument, we performed numerical simulations using the 1D radiative hydro-code MULTI. As shown in Figure 12, a shock is created in the CH ablator (zone 0), propagates through the aluminum (zones 1 and 3), then through the foam (zones 2 and 4). The interface between zones 2 (unshocked foam) and 4 (shocked foam) follows a straight line, which means that the shock speed is quasi constant along all the foam thickness.

The results that we have obtained for different foam densities are summarized in Figures 13, 14, and 15. The errors on the measured shock speeds include the errors on foam thickness, shock breakout time, and streak camera sweep speed. All other errors are deduced using the Rankine–Hugoniot relations.

Our EOS data are compared to those deduced from the SESAME tables for plastic (No. 7592). Indeed, this table

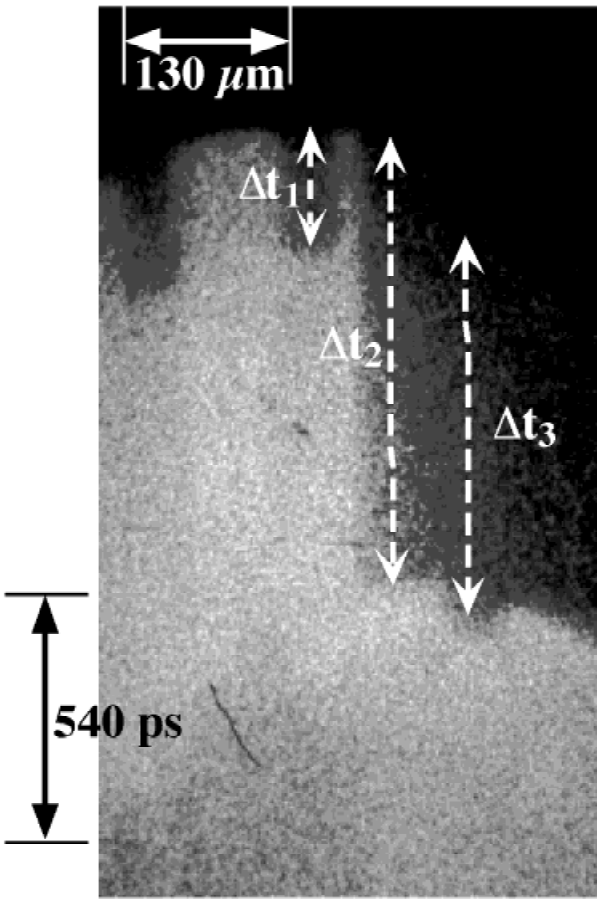


**Fig. 11.** Typical streak image of an EOS target. The target characteristics are: Al base = 8.9 $\mu$m, Al step = 5.5 $\mu$m, foam thicknesses = 23.8, and 29.3 $\mu$m. The laser intensity was $5 \cdot 10^{13}$ W/cm$^2$.

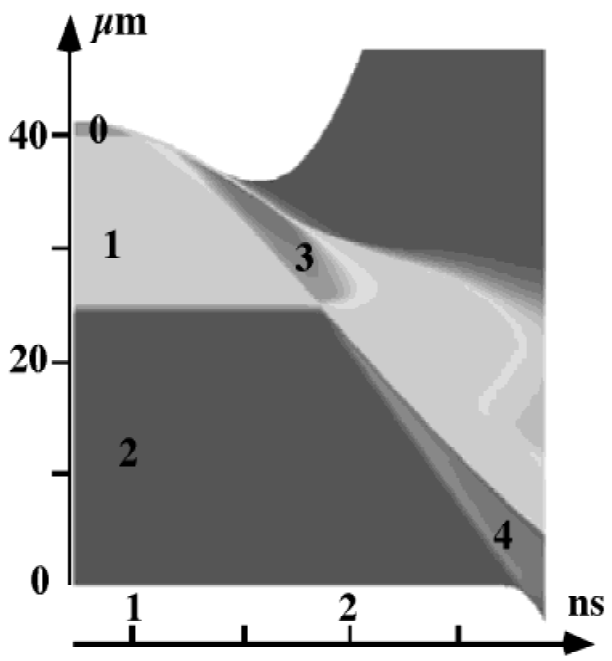


**Fig. 12.** Evolution of density versus time given by 1D simulations: zone 0: plastic ablator (1.04 g/cm$^3$); zone 1: initial aluminum density (2.7 g/cm$^3$); zone 2: initial foam density (200 mg/cm$^3$); zone 3: shocked aluminum; zone 4: shocked foam.

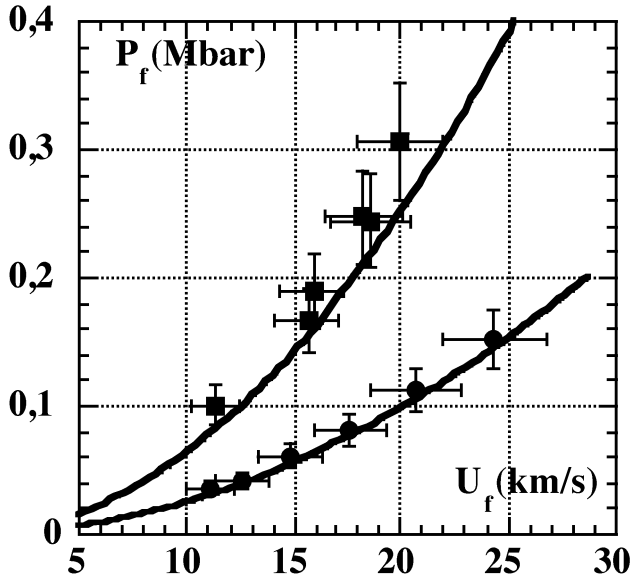


**Fig. 13.** Comparison between experimental data and SESAME Hugoniots in the ($P$, $U$) plane. The symbols ● and ■ are for 20- and 50-mg/cm$^3$ data points, respectively.

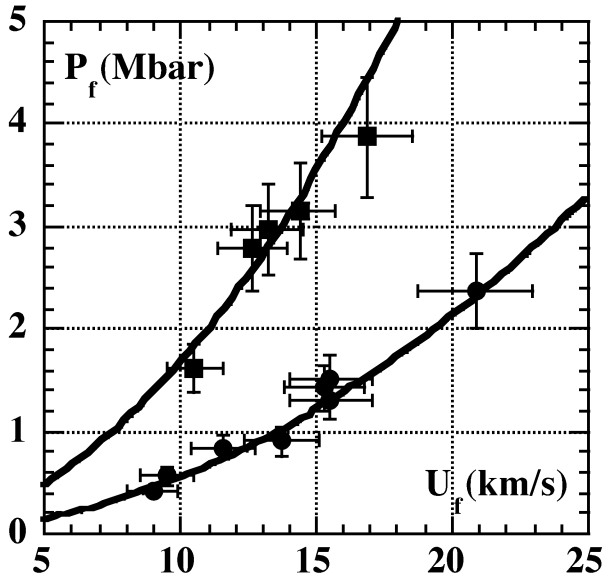


**Fig. 15.** Comparison between experimental data and SESAME Hugoniots in the ($P$, $U$) plane. The symbols ● and ■ are for 400- and 1100-mg/cm$^3$ data points, respectively.

has been specially adapted to fit some data points obtained for a 300-mg/cm$^3$ foam. We also checked that the SESAME table and calculations made with the Quotidian Equation of State (QEOS) model (More *et al.*, 1988) are very close (less than our error bars).

In Figure 13, for example, we compare our results for 20- and 50-mg/cm$^3$ foam, in the (P, U) plane, with the SESAME tables. As we can see, there is a satisfactory agreement, within the error bars, between our results and the theoretical curves. However there is a general deviation between experiment and theory, our data being more often above the Hugoniot curve, especially for the 50-mg/cm$^3$ case. Several reasons can explain this trend. First, the models (SESAME or QEOS) used for comparison may not reflect the exact characteristics of our material, in particular its chemical bonding, which might be important. Second, there could be a slight preheating of the foam due to the X rays created in the hot plastic ablator.

However according to recent work (Hall *et al.*, 1997; Benuzzi *et al.*, 1998*a*), the expected preheating level of the aluminum rear side is lower than 0.1 eV due to our moderate laser intensity $I \sim 6 \cdot 10/\mathrm{cm}^{13}$ W/cm$^2$. Since the X rays will propagate through a less absorbing medium (the foam being a low $Z$ material), one can expect that its effective preheating level is lower than this value. Such typical initial temperature ($\approx$0.1 eV) moves the Hugoniot curve a little bit off the principal one, toward the lower densities, which could explain part of the difference. Nevertheless, the only EOS data point published (to our knowledge) for low density foam (Holmes, 1991, 1994) is also very far from those tables, even if the error bars in this case are quite small (less than 1–2%).

In conclusion, we have developed original EOS measurements of porous materials with a moderate size laser ($E \sim$ 100 J). Results for five different foam densities and for plastic at normal density have been obtained for the first time with a laser in the 0.1–2.5 Mbar regime.

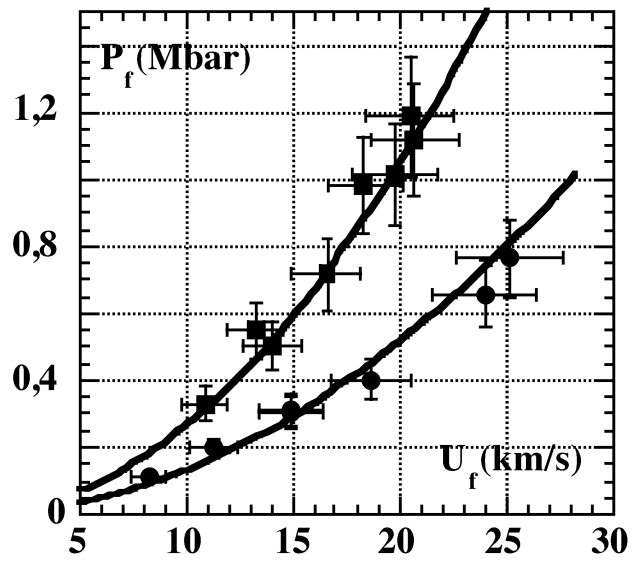


**Fig. 14.** Comparison between experimental data and SESAME Hugoniots in the ($P$, $U$) plane. The symbols ● and ■ are for 100- and 200-mg/cm$^3$ data points, respectively.

## 7. SHOCK ACCELERATION

Foams also play an important role in current astrophysical dedicated experiments. For example, these materials have been recently used to study the interaction of exploding star

ejecta with the circumstellar matter to simulate supernovae remnants formation (Remington *et al.*, 1997; Drake *et al.*, 1998). Also, porous materials allow the study of supercritical radiative shocks, which are of great importance in many astronomical objects such as exploding stars, and galactic or accretion discs. This is due to the large heating of the foam itself induced by compression and to the long mean free path of radiation in the low density material.

In this context, we studied the process of shock wave acceleration in a decreasing density profile. Sharp density gradients can be found in the outer atmosphere of many (if not all) stellar objects. This can be usually well approximated by an exponential decrease of the density spanning several orders of magnitude. Such exponential profiles are also found in accretion discs onto compact objects, such as black holes or neutrons stars, but also in galactic discs. If a shock wave propagates into such a sharply decreasing density profile, it gets accelerated very efficiently. This strong acceleration results in higher and higher postshock temperatures, in some cases up to the radiative regime. In supernovae explosions, this strong shock acceleration is supposed to give birth to a strong XUV burst, as the shock wave breaks out of the star surface (Falk, 1978; Woolsey, 1993). Moreover, such an accelerating configuration is known to be unstable to transverse perturbations of the shock front (Chevalier, 1990; Luo & Chevalier, 1994). This so-called "corrugation instability," caused by the decreasing density profile and the resulting shock acceleration, is believed to create density perturbations in the postshock flow, which are the seeds for the Rayleigh–Taylor instability at the interface between the star ejecta and the interstellar medium (Remington *et al.*, 1997; Drake *et al.*, 1998).

Creating a continuous, exponentially decreasing density profile within a laser experiment was beyond the scope of our initial measurements in which we only addressed the possibility to simulate a decreasing density profile using discrete density steps, and to obtain a strong shock acceleration with such a package.

The acceleration measurements were performed using the same experimental setup and the same kind of targets used for the foam EOS experiments described in the previous section. Data on shock acceleration at the aluminum–foam interface were obtained for a wide range of densities, from 20 mg/cm$^3$ up to 1.1 g/cm$^3$ and compared to a simple semianalytical model.

When the shock is transmitted from the denser Al layer to the lower density foam, the pressure decreases but the shock is highly accelerated. From our experimental results, we could infer the shock acceleration, that is, the ratios $U_f/U_{\mathrm{Al}}$ and $D_f/D_{\mathrm{Al}}$. Note that these parameters were determined without knowing the foam EOS. These results can then be compared to the classical problem of a shock hitting a step down discontinuity (Riemann problem) which admits a semianalytical solution for the acceleration in the case of a perfect gas EOS. Indeed, in this case, the polar curves for Al and for the foam are respectively given by

$$P = \frac{\gamma_{\mathrm{Al}} + 1}{2}\,\rho_{\mathrm{Al}} U^2$$

$$P = \frac{\gamma_f + 1}{2}\,\rho_f U^2. \tag{7}$$

The isentrope, originating from the experimental point $(P_{\mathrm{Al}}, U_{\mathrm{Al}})$, can be deduced using the perfect gas relations. It leads to the following equation:

$$U = U_{\mathrm{Al}} + \frac{2}{\gamma_{\mathrm{Al}} - 1}\, C_{\mathrm{Al}} \left[ 1 - (P/P_{\mathrm{Al}})^{\frac{\gamma_{\mathrm{Al}} - 1}{2\gamma_{\mathrm{Al}}}} \right] \tag{8}$$

where $C_{\mathrm{Al}}$ and $\gamma_{\mathrm{Al}}$ are the sound velocity and the adiabatic coefficient in the shocked aluminum, respectively. Then the intersection between the foam Hugoniot curve defined in Eq. (7) and the aluminum isentrope defined in Eq. (6) fixes the acceleration factor $g = U_g/U_{\mathrm{Al}}$ as the solution of the equation:

$$g = 1 + \sqrt{\frac{2\gamma_{\mathrm{Al}}}{\gamma_{\mathrm{Al}} - 1}} \left[ 1 - (Ag^2)^{\frac{\gamma_{\mathrm{Al}} - 1}{2\gamma_{\mathrm{Al}}}} \right] \tag{9}$$

where $A$ is given by

$$A = \rho_f(\gamma_f + 1)/(\rho_{\mathrm{Al}}(\gamma_{\mathrm{Al}} + 1)). \tag{10}$$

As pointed out in Koenig *et al.* (1999*c*), the acceleration factor $g$ is mainly a function of the density ratio $\rho_{\mathrm{Al}}/\rho_f$ for a step discontinuity $(\rho_{\mathrm{Al}}/\rho_f)$ greater than $10^3$. In our case, where $\rho_{\mathrm{Al}}/\rho_f$ is greater than this value, we expect that $g$ will depend weakly on the pressure at the interface.

From streak camera images like that of Figure 11, one can deduce the shock velocities. The acceleration factor $g$ in that case was equal to 1.4. All the results that we have obtained for different foam densities are summarized in Figure 16. Our experimental data are compared with the semianalytical model described above.

Our data are well described by the model and fit better with the same adiabatic coefficients for aluminum and for the foam ($\gamma_f = \gamma_{\mathrm{Al}} = 5/3$). However, the errors obtained on the measured shock velocities, as described before, are bigger than the difference between the two theoretical curves. The maximum acceleration factor obtained, in the case of the 20 mg/cm$^3$ foam, is $\approx$2.1. We found a slight dependence of the acceleration factor on laser intensity. Indeed, the points obtained for weak intensities ($I \leq 10^{13}$ W/cm$^2$) are all situated above the calculated acceleration factors. This trend is in good agreement with an acceleration factor calculated with the SESAME tables. It reflects the fact that the strong shock assumption of the model becomes partly nonvalid.

In conclusion, our results shows that the acceleration factor $g$ is almost insensitive to the initial pressure in aluminum as predicted by a simple model. The technique will allow further investigations, either with a two-step discontinuity,

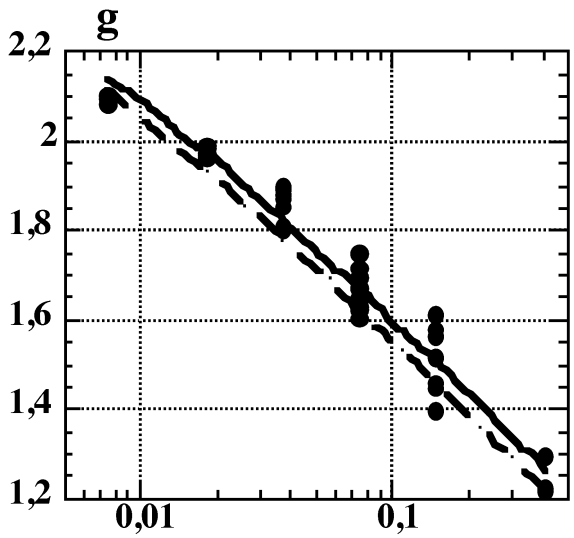


**Fig. 16.** Acceleration factor $g$ versus density ratio: ●: experimental results, (-----): perfect gas EOS model with $\gamma_{Al} = \gamma_f = 5/3$, and (——) with $\gamma_{Al} = 5/3$ and $\gamma_f = 1.2$.

in order to reach a typical acceleration factor of 3, or with a continuous decreasing density gradient.

## 8. CONCLUSIONS

The experimental works presented in this article, and many others cited in the references, shows how the use of low density foams may be a very useful means of realizing new experiments in the laser–plasma domain, which are of interest for ICF, EOS, and astrophysics. Fundamental to the success of such experiments are the use of uniform foams with submicron pore size, the use of optical smoothing techniques (PZP), and the use of space and time-resolved diagnostics. Other experiments will follow giving more insight into these new physical problems.

## ACKNOWLEDGMENTS

The experimental works were performed at LULI and MPQ and supported by the European Union program "Access to Large Scale Facilities." We thank all the physicists who have contributed to the work described here, namely: D. diSanto, L. Muller, F. Torsiello (Università di Milano–Bicocca), B. Faral, M. Temporal (LULI), and Th. Löwer (MPQ). For the work on shock acceleration, we are indebted to R. Teyssier (CEA) B. Remington and D. Ryutov (LLNL). Finally we warmly acknowledge the support of the LULI and MPQ technical teams during the experiment.

## REFERENCES

Batani, D. *et al.* (1995). *Laser Part. Beams* **14**, 211.
Batani, D. *et al.* (1998). *Plasma Phys. Control. Fusion* **40**, 1567.
Batani, D. *et al.* (1999). X-ray diagnostic applied to the study of shock wave propagation in foams. *Rev. Sci. Instrum.* **70**, 1464.
Batani, D. *et al.* (2000). *Phys. Rev. E* **62**, 8573.
Batani, D. *et al.* (2001). *Phys. Rev. E* **63**, 46410.
Benuzzi, A. *et al.* (1996). *Phys. Rev. E* **54**, 2162.
Benuzzi, A. *et al.* (1998*a*). *Phys. Plasmas* **5**, 2410.
Benuzzi, A. *et al.* (1998*b*). *Phys. Plasmas* **5**, 2827.
Bett, T. *et al.* (1995). *Appl. Opt.* **34**, 4025.
Cauble, R. *et al.* (1993). *Phys. Rev. Lett.* **70**, 2102.
Chaker, M. *et al.* (1988). *J. Appl. Phys.* **63**, 892.
Chevalier, R.A. (1990). *Astrophys. J.* **359**, 463.
Cohen, J.S. & Clark, R.H. (1996). Los Alamos Report LA-UR-96-3629, Los Alamos, NM: Los Alamos National Laboratory.
Collins, G. *et al.* (1998). *Science* **281**, 1178.
Cottet, F. *et al.* (1984). *Phys. Rev. Lett.* **52**, 1884.
Cottet, F. *et al.* (1985). *Appl. Phys. Lett.* **47**, 678.
Desselberger, M. *et al.* (1992). *Phys. Rev. Lett.* **68**, 1539.
Desselberger, M. *et al.* (1995). *Phys. Rev. Lett.* **74**, 2961.
Dixit, S. *et al.* (1994). *ICF Quarterly Report* vol. 4, p. 152. Livermore, CA: Lawrence Livermore National Laboratory.
Drake, P. *et al.* (1998). *Phys. Rev. Lett.* **81**, 2068.
Dunne, M. *et al.* (1995). *Phys. Rev. Lett.* **75**, 3858.
Eidmann, K. & Kishimoto, T. (1986). *Appl. Phys. Lett.* **49**, 377.
Emery, M.H. *et al.* (1991). *Phys. Fluids B* **3**, 2640.
Emery, M. & Gardner, J. (1992). *NRL Report* NRL/MR/6440-92-7170.
Fabbro, R. (1982). Etude de l'influence de la longeur d'onde laser sur les processus de conduction thermique et d'ablation dans les plasmas crees par laser. Thèse d'Etat, Université de Paris Sud.
Fabbro, R. *et al.* (1986). *Laser Part. Beams* **4**, 413
Fabbro, R. *et al.* (1990). *J. Appl. Phys.* **68**, 775.
Falconer, J. *et al.* (1994). *J. Vac. Sci. Technol. A* **2**, 2798.
Falconer, J. *et al.* (1995). *J. Vac. Sci. Technol. A* **13**, 1941.
Falk, S.W. (1978). *Astrophys. J. Lett.* **225**, 133.
Faral, B. *et al.* (1990). *Phys. Fluids B* **2**, 371.
Faral, B. *et al.* (1994). *Rapport Scientifique LULI 1993*, p. 309.
Gardner, J.H. & Bodner, S.E. (1981). *Phys. Rev. Lett.* **47**, 1137.
Hall, T. *et al.* (1997). *Phys. Rev. E* **55**, R6356.
Hoarty, D. *et al.* (1997). *Phys. Rev. Lett.* **78**, 3322.
Holmes, N. (1991). *Rev. Sci. Instrum.* **62**, 1990.
Holmes, N. (1994). In *APS Topical Conference on Shock Compression of Condensed Matter*, vol. 1, p. 153. Colorado Springs, CO: American Institute of Physics.
Kato, Y. *et al.* (1984). *Phys. Rev. Lett.* **53**, 1057.
Koenig, M. *et al.* (1994). *Phys. Rev. E* **50**, R3314
Koenig, M. *et al.* (1995). *Phys. Rev. Lett.* **74**, 2260.
Koenig, M. *et al.* (1998). *Appl. Phys. Lett.* **72**, 1033
Koenig, M. *et al.* (1999*a*). *Phys. Plasmas* **6**, 3296.
Koenig, M. *et al.* (1999*b*). *Appl. Phys. Lett.* **75**, 3026.
Koenig, M. *et al.* (1999*c*). *Appl. Phys. Lett.* **75**, 3026.
Lehmberg, R.H. & Obenschain, S.P. (1983). *Opt. Commun.* **46**, 27.
Lindl, J. (1995). *Phys. Plasmas* **2**, 3933.
Lower, Th. *et al.* (1994). *Phys. Rev. Lett.* **72**, 3186.
Luo, D. & Chevalier, R.A. (1994). *ApJ* **435**, 815.
Manheimer, W.M. *et al.* (1982). *Phys. Fluids* **25**, 1644.
Massen, J. *et al.* (1994). *Phys. Rev. E* **50**, 5130.
Mochizuki, T. *et al.* (1986). *Phys. Rev. A* **33**, 525.
Mora, P. (1982). *Phys. Fluids* **25**, 1051.
More, R.M. *et al.* (1988). *Phys. Fluids* **31**, 3059.

Nazarov, W. *et al.* (1998). *J. Moscow Phys. Soc.* **8**, 257.
Nazarov, W. *et al.* (1999). *Laser Part. Beams* **17**, 519.
Obenschain, S.P. *et al.* (1983). *Phys. Rev. Lett.* **50**, 44.
Ramis, R. *et al.* (1988). *Comput. Phys. Commun.* **49**, 475.
Remington, B. *et al.* (1997). *Phys. Plasmas* **4**, 1994.
Sckupsky, S. *et al.* (1989). *J. Appl. Phys.* **66**, 3456.
Stevenson, R.M. *et al.* (1994). *Optics Lett.* **19**, 363
Taylor, R.J. *et al.* (1996). *Phys. Rev. Lett.* **76**, 1643.
Trainor, R.J. *et al.* (1978). *Phys. Rev. Lett.* **42**, 1154.
T4 Group. (1983). *SESAME Report on the Los Alamos Equation-of-State Library*, Report No. LALP-83-4. Los Alamos, NM: Los Alamos National Laboratory.
van Kessel, C.G.M. & Sigel, R. (1974). *Phys. Rev. Lett.* **33**, 1020.
Veeser, L.R. & Solem, S.C. (1978). *Phys. Rev. Lett.* **40**, 1391.
Woolsey, S.E. (1993). *Astron. Astro*., **97**, 205.
Zeldovich, Y.B. & Raizer, Y.P. (1967). *Physics of Shock Waves and High Temperature Hydrodynamic Phenomena*. New York: Academic Press.